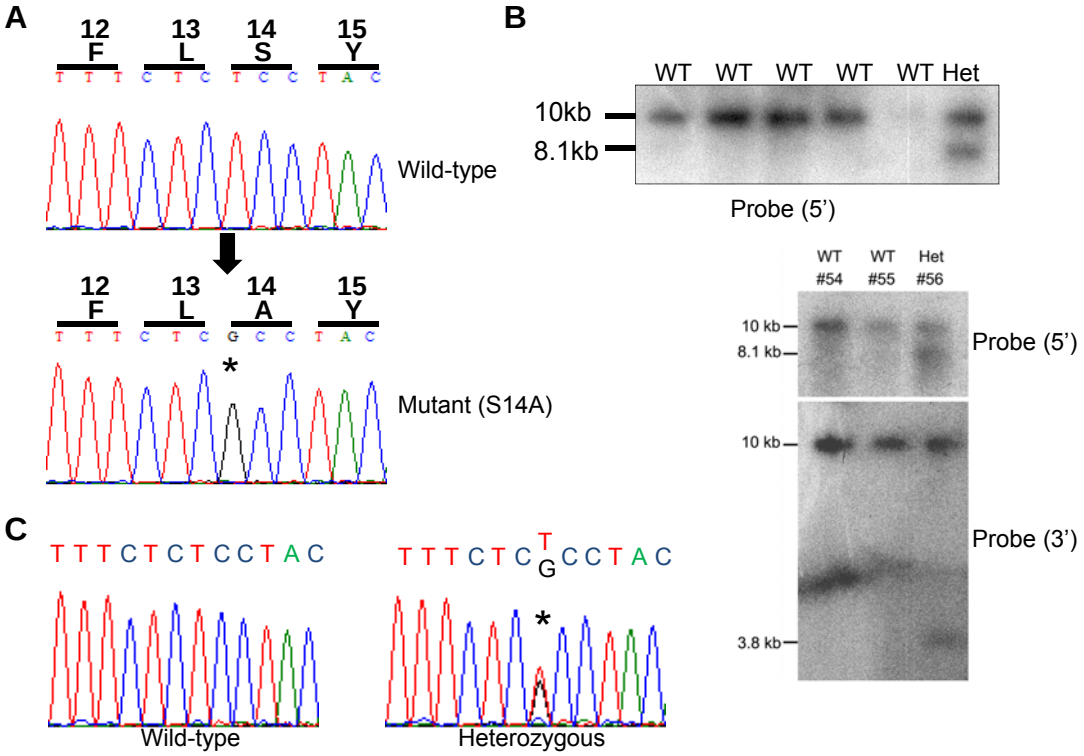

Supplemental Figure 1 Generation of Bcl-xL phosphorylation mutant (S14A) knock-in mice. (**A**) S14A mutation in targeting construct was confirmed by sequencing analyses. (**B**) DNA isolated from Neo-resistant ES clones was digested with *MfeI* and assessed by Southern blotting for wild-type (WT) and heterozygous (Het) alleles with the probes shown in Fig 1(*A*). (**C**) Incorporation of S14A mutation in positive ES clones was verified by PCR and sequencing analyses. Mutations are highlighted by asterisks.

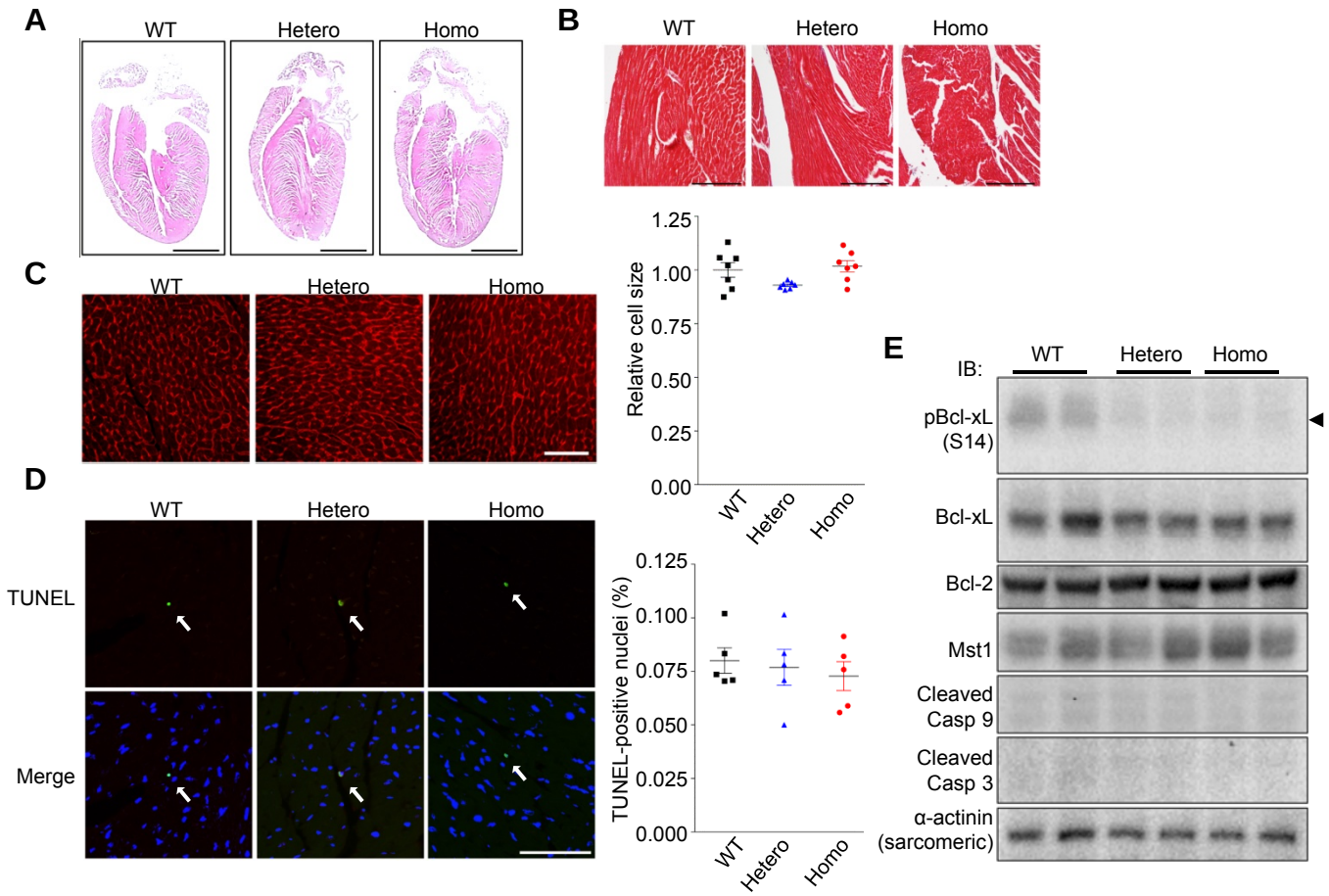

Supplemental Figure 2 Characteristics of Bcl-xL S14A KI mice. (**A**) Hematoxylin-Eosin staining of transverse sections of hearts obtained from the indicated 11 to 12-week-old mice. Scale bar, 2 mm. (**B**) Representative heart sections from the indicated mice, stained with Masson's Trichrome. Scale bar, 100 μm. (**C**) Representative WGA staining in indicated mice showing cardiomyocyte cell size (left, scale bar, 50 μm) and quantification of relative cell size (n=5 each) (right). (**D**) Representative TUNEL (green) and nuclear (blue) staining in indicated mice (left, scale bar, 50 μm) and quantification of TUNEL-positive nuclei (%) (right). White arrows indicate TUNEL-positive nuclei. (**E**) Immunoblots showing phosphorylation of Bcl-xL at Ser14, Bcl-2, Mst1, and cleaved caspases. Data are mean±SEM.

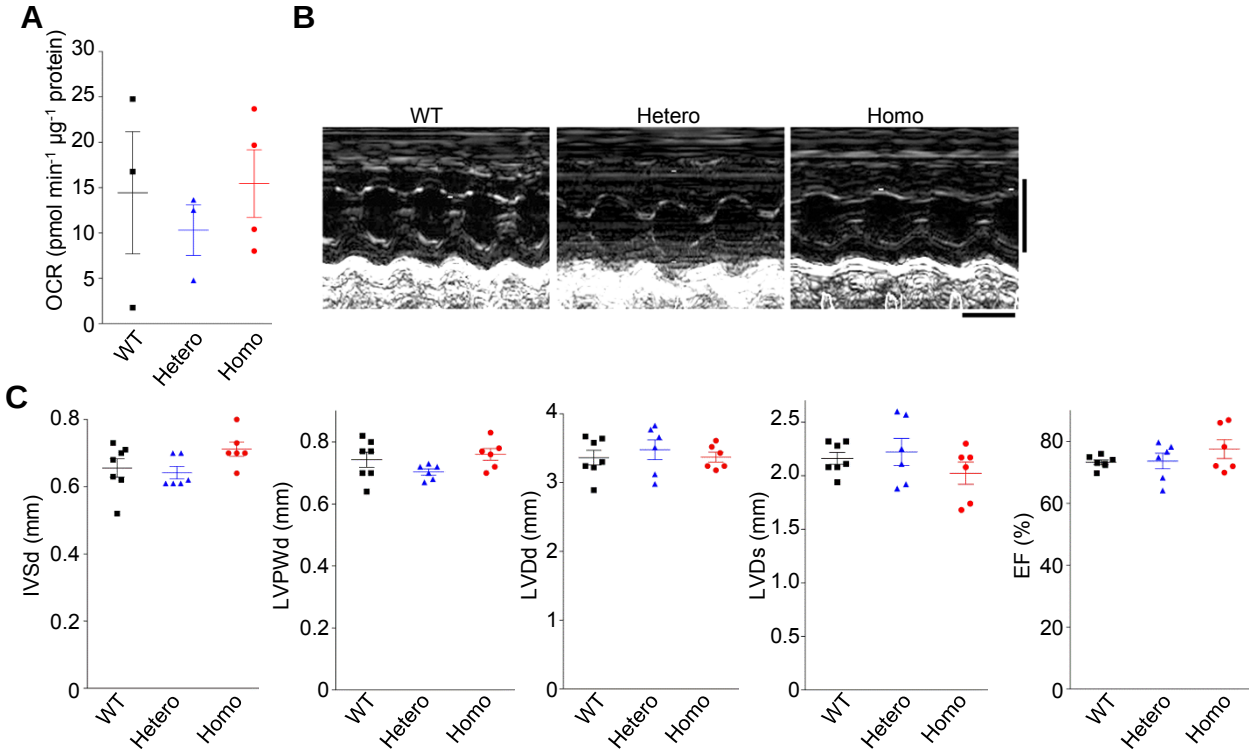

Supplemental Figure 3 Mitochondrial and cardiac function of Bcl-xL S14A KI mice. (**A**) Basal oxygen consumption rate (OCR) using mitochondria isolated from the indicated mice (n = 3-4). (**B**) Representative images showing M-mode echocardiography. Transverse scale bar, 100 ms. Vertical scale bar, 5 mm. (**C**) Echocardiographic analyses of cardiac morphology and function. IVSd, interventricular septal thickness at diastole; LVPWd, left ventricular (LV) posterior wall dimension at diastole; LVDd, LV end-diastolic dimension; LVDs, LV end-systolic dimension; EF, ejection fraction (n = 6-7).

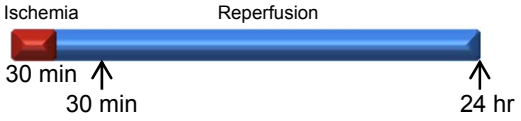

Supplemental Figure 4 Schematic representation of I/R experiment. Heart samples were harvested after 30 minutes of reperfusion for protein expression analyses or 24 hours of reperfusion for measuring infarct size and TUNEL staining.

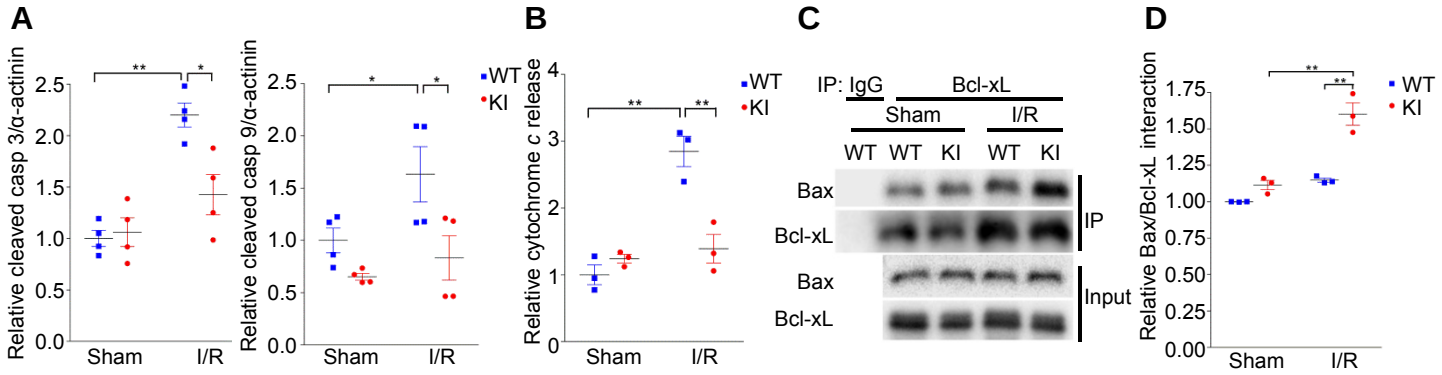

Supplemental Figure 5 S14A KI inhibits mitochondrial pathway of apoptosis. (**A**) Quantification of relative cleaved caspase 3 (left) and cleaved caspase 9 (right) expression in response to sham or ischemia-reperfusion surgery (n = 4 in each group). (**B**) Quantification analyses of cytochrome c release (n = 3). (**C**) Immunoblots showing interaction between Bcl-xL and Bax. Bax was co-immunoprecipitated with Bcl-xL. The data are representative of three independent experiments. (**D**) Quantification analyses of Bax co-immunoprecipitated with Bcl-xL (n = 3). Data are mean±SEM. * $p < 0.05$ and ** $p < 0.001$.

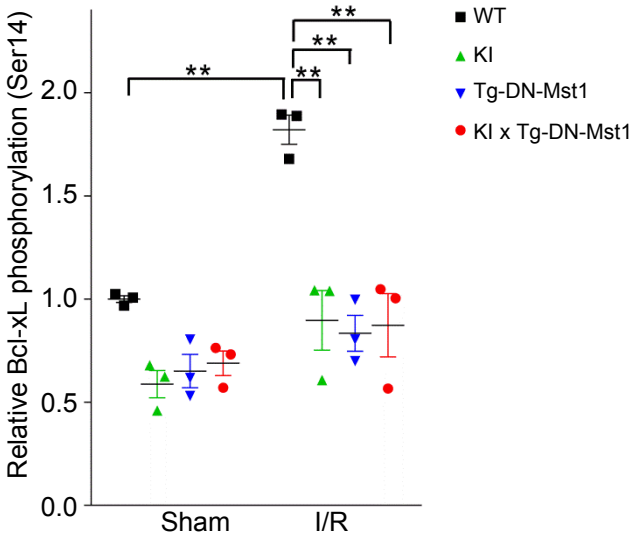

Supplemental Figure 6 Phosphorylation status of Bcl-xL (Ser14) in response to ischemia-reperfusion. Quantification of the relative phosphorylation of Bcl-xL-Ser14 in hearts of indicated mice subjected to sham or ischemia-reperfusion surgery (n = 4 in each group). Data are mean±SEM. * $p < 0.05$ and ** $p < 0.001$.

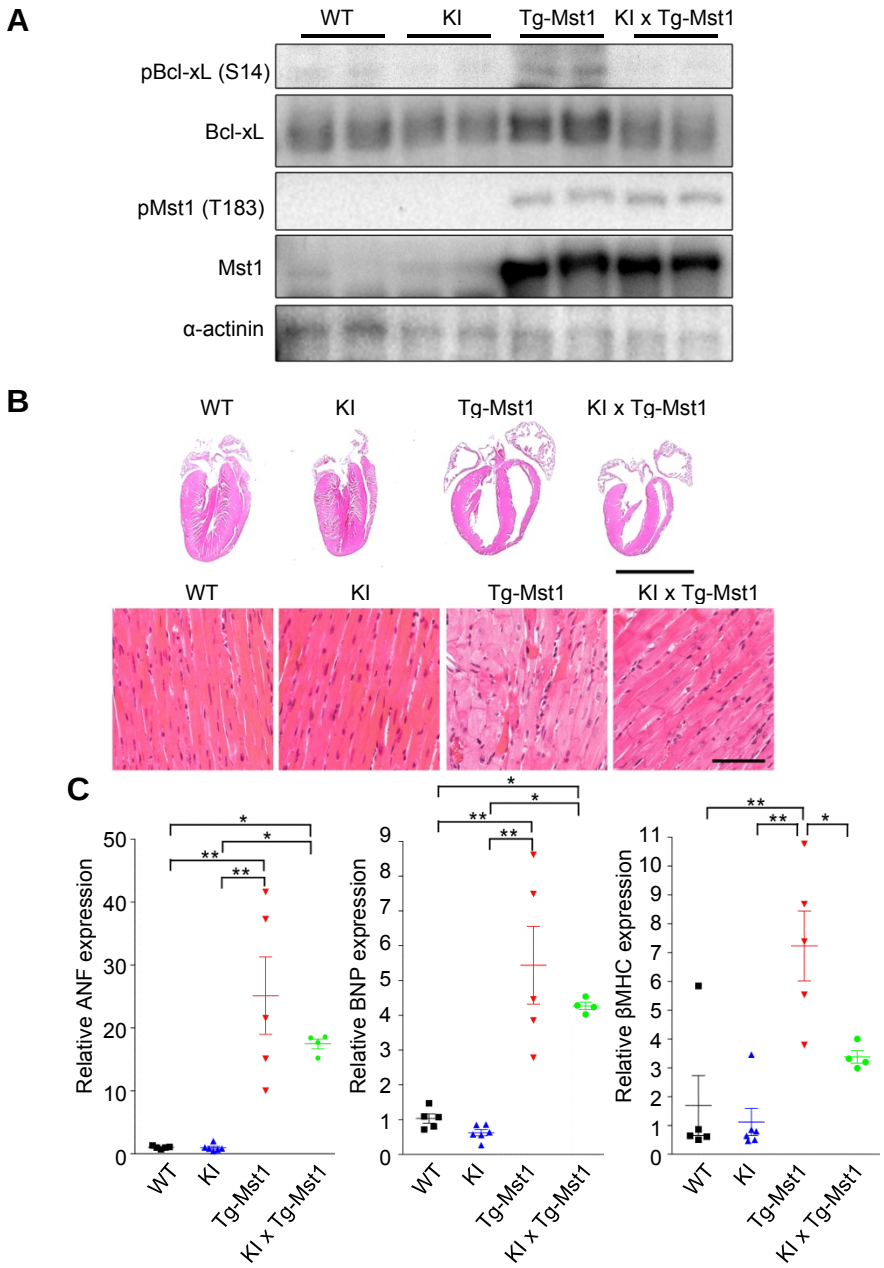

Supplemental Figure 7 Inhibition of Bcl-xL Ser14 phosphorylation attenuates Mst1-induced cardiomyopathy. (**A**) Immunoblots showing phosphorylation of Bcl-xL at Ser14 and Mst1. Phosphorylated Bcl-xL is increased in Tg-Mst1 mice, an effect that is normalized in bigenic mice. (**B**) Representative transverse heart sections (upper, scale bar, 5 mm) and higher magnification (lower, scale bar, 50 μm), stained with Hematoxylin-Eosin. (**C**) Relative mRNA expression of fetal-type genes, atrial natriuretic factor (ANF), brain natriuretic peptide (BNP), and β-myosin heavy chain (βMHC) (n = 4-6). Data are mean±SEM. * $p < 0.05$ and ** $p < 0.001$.

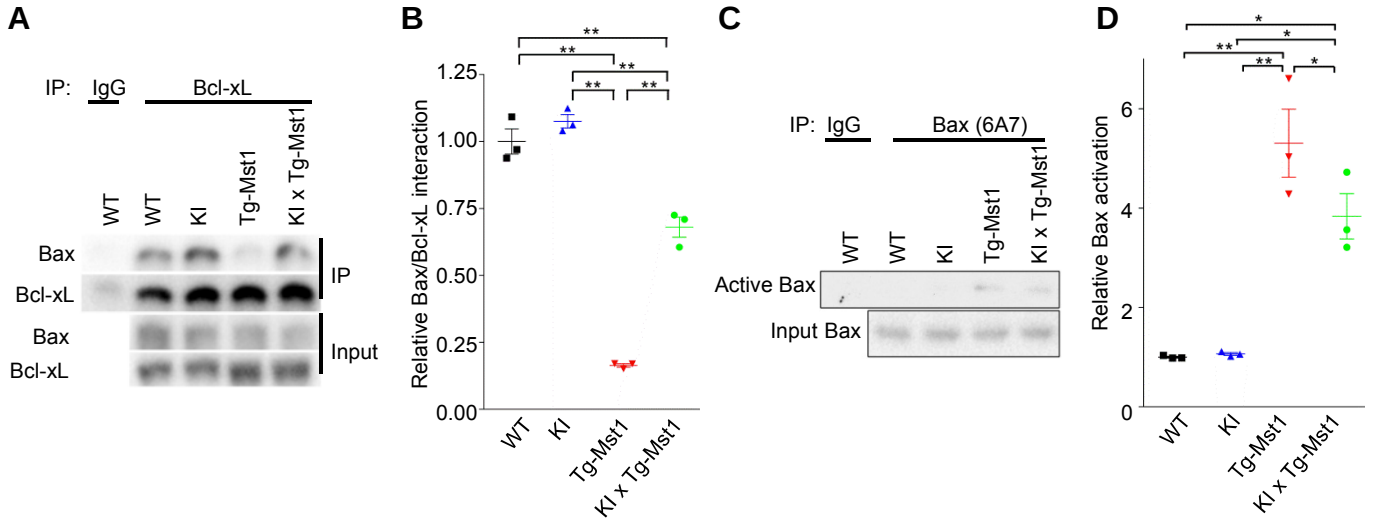

Supplemental Figure 8 Activation of Bax in Tg-Mst1 mice was ameliorated by Bcl-xL-S14A. (**A**) Immunoblots showing the interaction between Bax and Bcl-xL in indicated mice. Bax was co-immunoprecipitated with Bcl-xL. The data are representative of three independent experiments. (**B**) Quantification analysis of relative Bax interaction with Bcl-xL (n = 3). (**C**) Immunoblots showing active Bax (6A7). The data are representative of three independent experiments. (**D**) Quantification of relative Bax activation (n = 3). Data are mean±SEM. * $p < 0.05$ and ** $p < 0.001$.

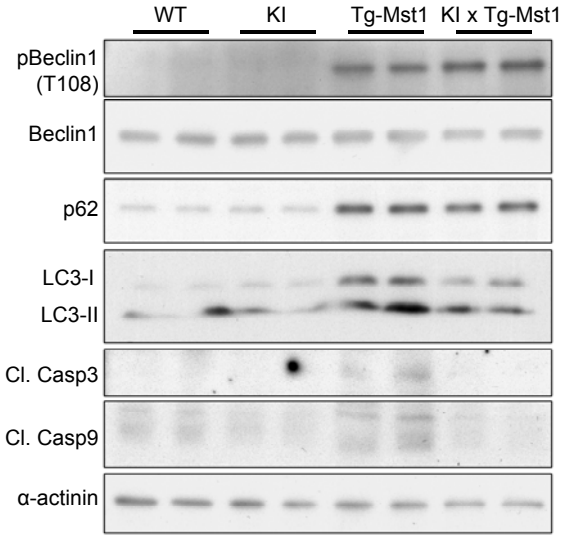

Supplemental Figure 9 Autophagy was inhibited in both Tg-Mst1 and bigenic mice generated by crossing KI and Tg-Mst1 mice. Immunoblots show phosphorylation of Beclin1 (T108), p62, LC3-I/II and Cleaved caspase 3 and 9. Mst1-mediated phosphorylation of Beclin1 at Thr108 was increased in both Tg-Mst1 and KI-Tg-Mst1 mice, accompanied by an increase in p62 accumulation.

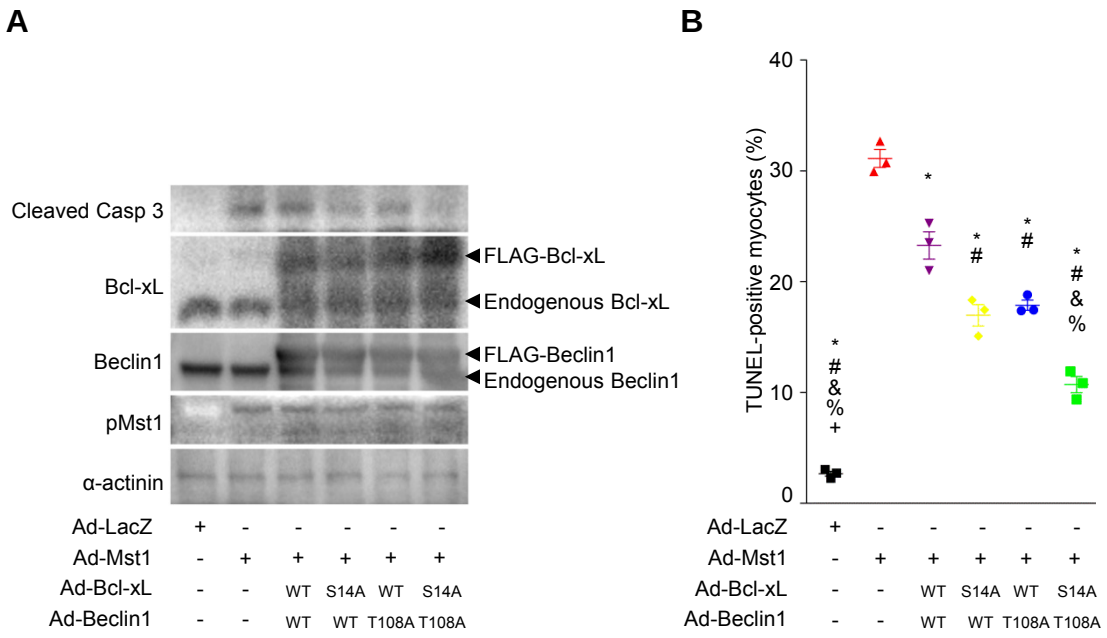

Supplemental Figure 10 Mst1-induced apoptosis was independently regulated by Bcl-xL and Beclin1. (**A**) Immunonlots show cleaved caspase 3 in response to Mst1 overexpression. Cardiomyocytes were transduced with adenovirus (Ad-) harboring LacZ or Ad-Mst1 in the presence or absence of Ad-Bcl-xL-WT or S14A and Ad-Beclin1-WT or T108A for 48hrs. (**B**) TUNEL-positive cardiomyocytes after transduction with the indicated adenovirus for 48 hours (n = 3 in each group).* $p < 0.001$ compared with Mst1 (red), # $p < 0.001$ compared with Mst1 & Bcl-xL-WT & Beclin1-WT (purple). & $p < 0.001$ compared with Mst1 & S14A & Beclin1-WT (yellow). % $p < 0.001$ compared with Mst1 & Bcl-xL-WT & T108A (blue). + $p < 0.001$ compared with Mst1 & S14A & T108A (green). Data are mean±SEM. ANOVA with Newman-Keuls post-hoc analysis.

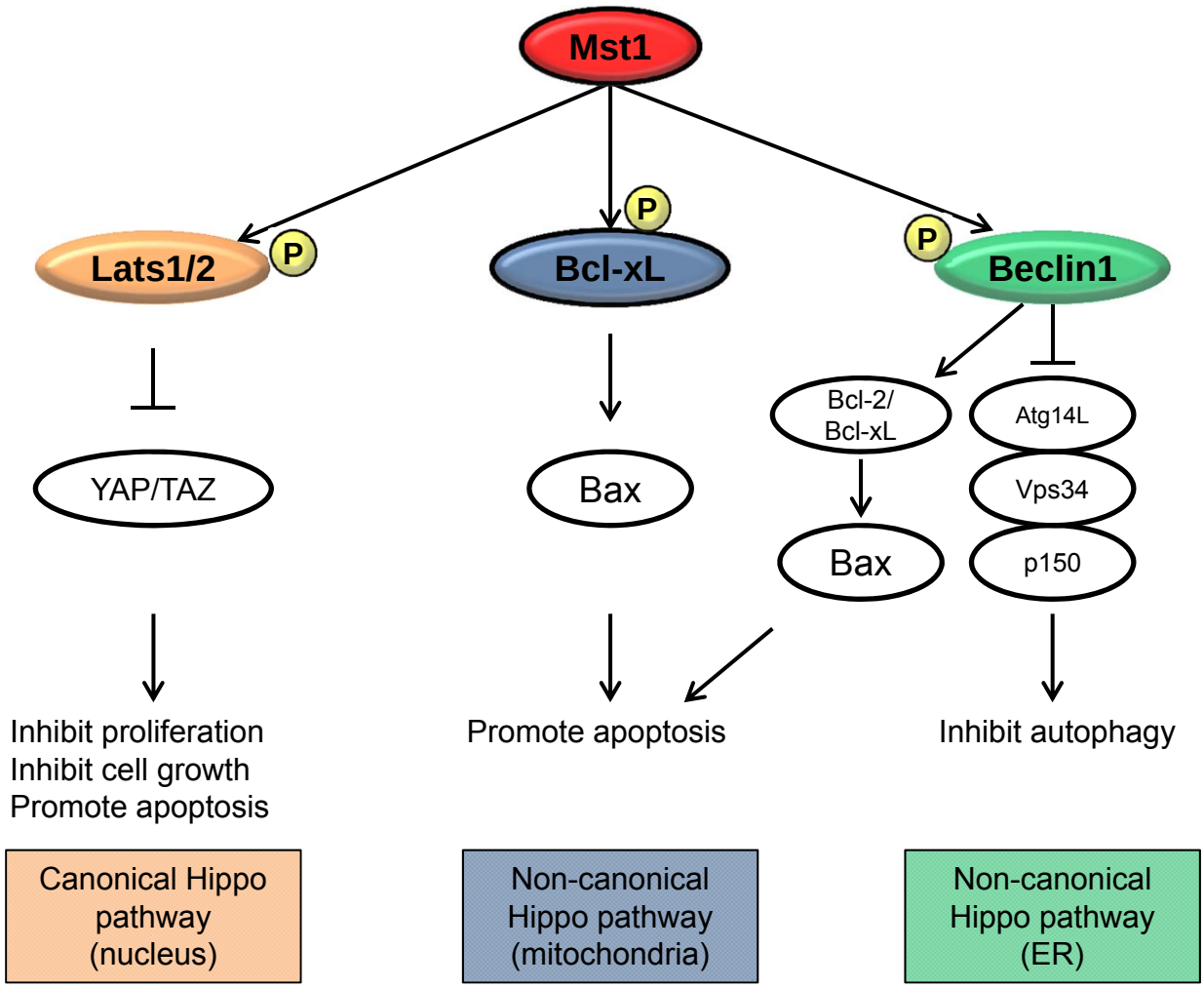

Supplemental Figure 11 Schematic representation of Mst1 signaling in the canonical and non-canonical Hippo pathways.

	Total #	WT	Hetero KI	Homo KI
Male	49	13 (26.5%)	24 (49.0%)	12 (24.5%)
Female	34	12 (35.3%)	16 (47.1%)	6 (17.6%)
Expected		25%	50%	25%

Supplemental Table 1 Offspring chart for mice crossed with heterozygous KI mice.

	WT (n = 5)	Hetero (n = 5)	Homo (n = 5)
Age (weeks)	11.6 ± 0.3	11.3 ± 0.3	11.6 ± 0.3
BW (g)	21.0 ± 0.4	21.2 ± 0.4	20.4 ± 0.2
LV (mg)	79.4 ± 2.0	78.8 ± 1.2	77.4 ± 0.9
RV (mg)	10.4 ± 0.5	11 ± 0.4	10.6 ± 0.7
LA (mg)	2.6 ± 0.2	2.8 ± 0.2	2.6 ± 0.2
RA (mg)	2.2 ± 0.2	2.4 ± 0.2	2.2 ± 0.2
Liver (mg)	925 ± 6.5	963.2 ± 30.9	949.6 ± 17.9
Lung (mg)	120.6 ± 4.5	113.6 ± 3.9	114.4 ± 2.3
LV/TL (mg/mm)	4.91 ± 0.12	4.86 ± 0.08	4.78 ± 0.06
Liver/TL (mg/mm)	57.2 ± 0.51	59.5 ± 1.92	58.7 ± 1.16
Lung/TL (mg/mm)	7.46 ± 0.28	7.01 ± 0.25	7.07 ± 0.13

Supplemental Table 2 Postmortem pathologic measurements of WT, heterozygous KI and homozygous KI mice. BW, body weight; LV, left ventricle; RV, right ventricle; LA, left atrium; RA, right atrium; TL, tibia length.